Analytica Chimica Acta: X 9 (2021) 100077

Contents lists available at ScienceDirect

Analytica Chimica Acta: X

journal homepage: www.sciencedirect.com/journal/analytica-chimica-acta-x

Electrochemical application of cobalt nanoparticles-polypyrrole composite modified electrode for the determination of phoxim

Molla Tefera [a,*], Merid Tessema [b], Shimelis Admassie [b], Meryck Ward [c], Lisebo Phelane [c], Emmanuel I. Iwuoha [c], Priscilla G.L. Baker [c]

[a] Department of Chemistry, University of Gondar, P. O. Box 196, Gondar, Ethiopia
[b] Department of Chemistry, Addis Ababa University, P. O. Box 1176, Addis Ababa, Ethiopia
[c] Sensor Lab, Department of Chemistry, University of the Western Cape, Private Bag X17, Robert Sobukwe Drive, Bellville, 7535, South Africa

ARTICLE INFO

Keywords:
Cobalt nanoparticles
Polypyrrole
Modified electrode
Phoxim
Water
Electrochemical sensor

ABSTRACT

In this study, cobalt nanoparticles (CoNPs) were synthesized and cobalt nanoparticles modified glassy carbon electrode (CoNPs/GCE) was prepared by drop coating the nanoparticles on glassy carbon electrode. After preparing polypyrrole modified glassy carbon electrode (PPy/GCE) using electropolymerization of pyrrole in $LiClO_4$ solution, cobalt nanoparticles-polypyrrole composite modified glassy carbon electrode (CoNPs/PPy/GCE) was fabricated by drop coating the CoNPs on the PPy/GCE. Different characterization techniques such as scanning electron microscopy, transmission electron microscopy, energy dispersive spectroscopy, FTIR spectroscopy, electrochemical impedance spectroscopy and cyclic voltammetry were used to study the morphological structure and electrochemical behavior of the sensors. The results demonstrated that PPy chains interacted with CoNPs through donor-acceptor bonds. Among all the electrodes, CoNPs/PPy/GCE exhibited highest electroactive surface area and lowest electron transfer resistance towards phoxim. Under the optimal conditions, the sensor showed linear relationship between the reduction peak current and the concentration of phoxim in the range of 0.025 μM–12 μM with the detection limit as 4.5 nM. Besides, the composite electrode demonstrated excellent reproducibility, good stability and selectivity towards the possible interfering substances. All of these properties made CoNPs/PPy/GCE a suitable electrochemical sensor for the electrochemical determination of phoxim in water samples using square wave voltammetry.

1. Introduction

Organophosphate (OP) pesticides are the most extensively used pesticides across the world in agriculture [1]. Due to highly persistence and toxicity, even trace contamination of organophosphorus pesticides in the environment and food chain creates a lot of pollution problems [2,3]. Their toxicities are caused by inhibiting the activity of acetylcholinesterase (an enzyme in the central nervous system), often leading to perturbation of nerve conduction system and paralysis the functions of living systems and finally leads to death [4,5].

Phoxim (phenylgloxylonitrile-oxime-o,odiethyl-phosphorothionate) is an organothiophosphate insecticide that is widely used to control a wide range of insect pests in fruits, vegetables and commercial crops [6]. High-performance liquid chromatography and high-performance liquid chromatography-mass spectrometry methods have been reported for the determination of phoxim residues [7,8]. However, these methods are expensive and require complicated instruments and qualified personnel. Recently, electrochemical methods have gained more interest for determination of pesticides due to various advantageous such as compact nature, easy to handle in field trials, low cost, higher sensitivity and selectivity [9,10].

Phoxim was determined electrochemically at the surface of gold nanoparticles and silk fibroin composite modified platinum electrodes [11], graphene–modified glassy carbon electrode [12], graphene oxide–gold nanocomposite modified glassy carbon electrode [13], poly (3-methylthiophene)–nitrogen doped graphene-modified glassy carbon electrode [14], molecular imprinting graphene modified glassy carbon electrode [15] and multiwalled carbon nanotube grafted acryloyloxy ferrocene carboxylates modified glassy carbon electrode [16].

Conducting polymers such as polyaniline, polypyrrole and polythiophene have been studied intensively during the last decades due to their high electrical conductivity, environmental stability and low cost.

* Corresponding author.
E-mail addresses: mollatef2001@gmail.com, molla.tefera@uog.edu.et (M. Tefera).

https://doi.org/10.1016/j.acax.2021.100077
Received 27 May 2021; Received in revised form 17 September 2021; Accepted 18 September 2021
Available online 21 September 2021

Besides high flexibility in preparation and good mechanical properties, polypyrrole has gained special interest in various applications [17,18]. Owing to promising high surface to volume ratio and structural property; good conductivity and excellent catalytic activity of nanomaterials, nanomaterials are widely applicable to enhance physical and mechanical properties of polymers [19]. Composite of nanomaterials and polymers exhibited much higher sensitivity and better selectivity than the pure inorganic and organic materials [20–22].

To the best of our knowledge, no literature reports on voltammetric determination of phoxim at CoNPs/PPy/GCE have been published. In this work, electrochemical sensors based on CoNPs/GCE, PPy/GCE and CoNPs/PPy/GCE were prepared and characterized using FTIR, high resolution scanning electron microscope (HRSEM), high resolution transmission electron microscope (HRTEM), electrochemical impedance spectroscopy and electrochemical methods. The experimental parameters were optimized in order to enhance the performance of CoNPs/PPy/GCE and it was applied for the determination of phoxim in water samples.

2. Experimental

2.1. Reagents

Cobalt chloride hexahydrate (Sigma Aldrich, 202185, 98%), pyrrole (Sigma Aldrich, 131709, 98%), phoxim (98%), sodium borohydride (98%), dichlorvos (98.8%), phenothrin (94.4%), magnesium sulphate (99.5%), ferric chloride hexahydrate (97%) and zinc nitrate hexahydrate (99%) were purchased from Sigma–Aldrich (Germany) and used as received. All other reagents were of analytical grade. A 0.1 M phosphate buffer solution (PBS) which was prepared using a mixture of KH_2PO_4 (99%) and K_2HPO_4 (98%) was employed as a supporting electrolyte. Pyrrole monomer was distilled under reduced pressure and stored in a refrigerator. Double distilled water was used throughout the experiment. The phoxim standard solution was dissolved in ethanol and was stored in a refrigerator. The working solutions of phoxim were prepared by diluting the stock solution with PBS.

2.2. Apparatus and instrumentation

All voltammetric measurements were carried out using PalmSens Trace (Palm Instruments BV, Utrecht, Netherlands) connected to a personal computer. The measurements were performed by employing three electrode system with GCE (3.0 mm diameter, Sigma Aldrich, Germany), CoNPs/GCE, PPy/GCE and CoNPs/PPy/GCE working electrodes, silver-silver chloride electrode (3 M NaCl) reference and platinum wire (1.0 mm diameter) counter electrode. Electrochemical impedance spectroscopic measurements (EIS) were performed on a CHI604D electrochemical workstation (CH Instruments, Inc., Austin, Texas, USA). FTIR spectra were recorded on a PerkinElmer Spectrum 100-FTIR spectrometer (Waltham, USA).

The morphology and elemental compositions of PPy, CoNPs and CoNPs/PPy composite were examined using high resolution scanning electron microscopy (AURIGA, Field Emission Gun High Resolution Scanning Electron Microscope (FEG HRSEM, Zeiss), high resolution transmission electron microscopy (HRTEM, FEI Tecnai G2 F20 X-Twin 200 kV field-emission gun) and energy dispersive spectroscopy.

For HRSEM measurement, screen printed carbon electrodes were used for electrodeposition of PPy, CoNPs and CoNPs/PPy composite. However, HRTEM measurements the samples were prepared by drop coating one drop of specimen solution onto a holey carbon coated copper grid. Then, it was dried under a Xenon lamp for about 10 min, where after, the coated grids were analyzed under the microscope.

2.3. Synthesis of cobalt nanoparticles

Synthesis of cobalt nanoparticles was performed according to the procedure proposed by Phelane et al. [23]. Briefly, 0.5 M solution of CoCl2·6H2O solution was prepared by dissolved it in ethanol. To this solution, a mixture of 1.0 M NaBH4 and 0.2 M NaOH was added. The resulting solution was allowed to stay for 24 h until the reaction was completed. Then after, the solution was centrifuged for 20 min and the precipitate was washed completely with double distilled water and ethanol. Finally, the precipitate was dried in an oven for 24 h and ground with a pestle and mortar.

2.4. Preparation of CoNPs/PPy/GCE electrode

Before modification, the bare glassy carbon electrode was polished with different sizes (1.0, 0.3 and 0.05 μm) of alumina slurry in sequence until a mirror like surface was obtained and then it was washed with double distilled water. Finally, it was sonicated with ethanol and double distilled water successively in order to remove adsorbed particles, and then dried at room temperature. A 0.25 M solution of pyrrole in 0.10 M $LiClO_4$ was electropolymerized on GCE by cycling in the potential range −1.1 V–0.7 V at a scan rate of 0.05 V s^{-1} for 15 cycles for preparing PPy/GCE. Thereafter, CoNPs/PPy/GCE was prepared by drop coating 5 μL of CoNPs in dimethylformamide solution onto PPy/GCE surface and dried in air prior to analysis.

2.5. Sample preparation

For analytical application, water samples were collected from Kuils River, Cape Town, South Africa. In order to remove particulate matter, the water samples were filtered and stored in refrigerator for a week until analysis. To the water samples, ethanol was added and the pH value of water samples (2 mL) was adjusted with 5 mL of 0.1 M PBS of pH 6.0. The spiked sample solutions were prepared with the addition of various concentrations of phoxim standard solutions.

All electrochemical cells were purged with nitrogen gas for at least 10 min prior to all electrochemical measurements. All measurements were also performed at room temperature.

3. Results and discussion

3.1. Morphological and structural characterization CoNPs/PPy composite

During electropolymerization process, an oxidation peak was observed around 0.1 V in the forward scan, which corresponds to the formation of pyrrole radical cations (PPy^+). In the reverse scan, a reduction peak was appeared around −0.15 V due to the reduction of the pyrrole radical cations [24]. The increased in the intensity of the peak currents with increasing scanning cycles confirmed the formation of polypyrrole films on the surface of GCE (Fig. 1A). Therefore, the thickness of the polymer on the electrode could be controlled by the number of scans. Furthermore, the electrochemical behavior of the bare GCE and PPy/GCE were studied in a monomer free supporting electrolyte. As can be seen (Fig. 1B curve a), peaks were not observed at GCE. However, oxidation and reduction peaks appeared at 0.25 V and −0.32 V at PPy/GCE, respectively, indicating that the polypyrrole film was formed at the surface of the GCE (Fig. 1B curve b). Finally, CoNPs solution drop coated on the surface of the polymer film in order to produce CoNPs/PPy/GCE.

The interactions between CoNPs and PPy particles in the composite were investigated and supported by FTIR spectroscopy. Fig. 2 displays the FTIR spectra of PPy and CoNPs/PPy. For pure PPy, an absorption band at 3150 cm^{-1} was attributed to the N–H stretching vibration, absorption peaks at 1500 cm^{-1} and 1400 cm^{-1} were due to C═C and C–N stretching of pyrrole ring, respectively. The broad band around 1210 cm^{-1} was caused by the C–N stretching and = C–H in-plane deformation vibrations of the aromatic ring, while the two absorption peaks that appeared at 850 cm^{-1} and 620 cm^{-1} were due to C–H out-of-plane bending [25,26]. However, the FTIR spectrum of CoNPs/PPy shows

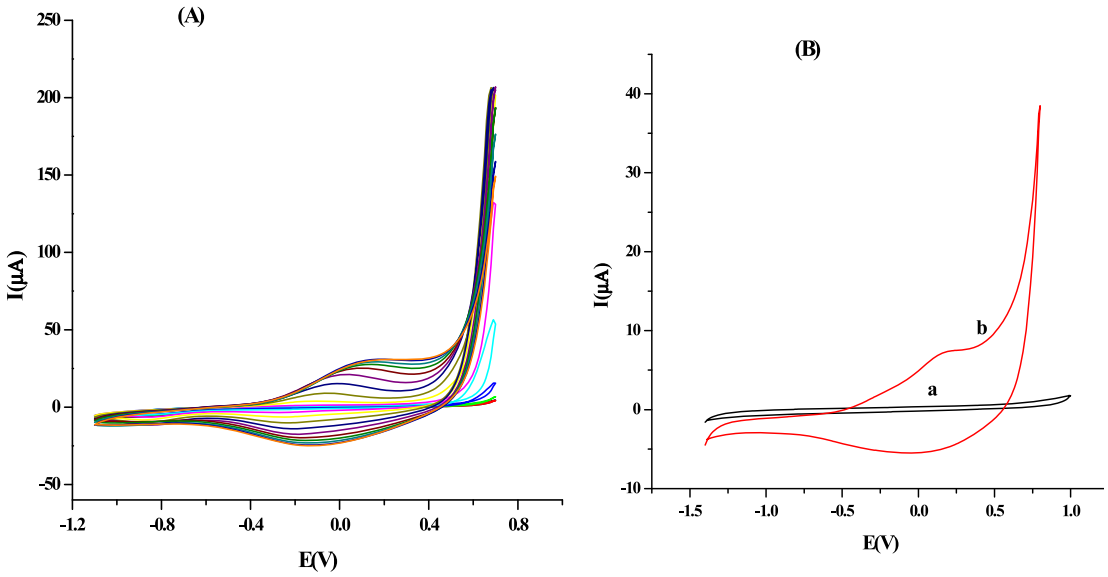

Fig. 1. Cyclic voltammograms of (A) electropolymerization of 0.25 M pyrrole in 0.10 M $LiClO_4$ and (B) a monomer free 0.10 M $LiClO_4$ on GCE (a) and PPy/GCE (b).

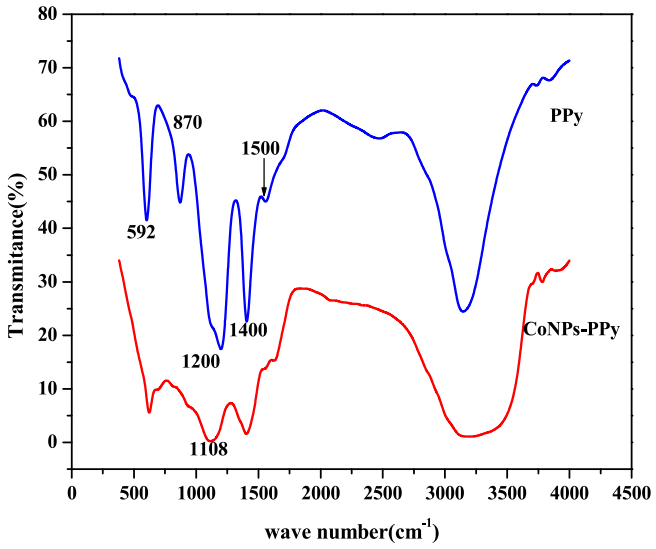

Fig. 2. FTIR spectra of PPy and CoNPs/PPy.

the characteristics peaks of PPy, with a shift of peak positions toward lower wave number (1400 cm^{-1} to 1390 cm^{-1} and 1200 cm^{-1} to 1108 cm^{-1}), indicating the dispersion of the electron density of PPy as a function of the incorporation of the nanoparticles [27].

From the spectral changes of FTIR, a strong coordination bond was formed between cobalt and the negatively charged (deprotonated) pyrrolic nitrogen (Scheme 1), which is in agreement with the structure proposed by Shi et al. [28].

The surface morphology of CoNPs, PPy and CoNPs/PPy was characterized using HRSEM and HRTEM analyses. The HRSEM spectra are presented in Fig. 3. The image of PPy showed non-uniform distribution of PPy particles. In CoNPs, the shape of grain particle is spherical and distributed uniformly. However, the HRSEM image at CoNPs/PPy showed the size of nanocomposites to be larger than CoNPs which reinforced the successful encapsulation of CoNPs within the PPy.

The inner structures of PPy, CoNPs and CoNPs/PPy composite were studied using high resolution transmission electron microscope (HRTEM). It can be seen that the sizes of the particles in CoNPs/PPy were bigger than in CoNPs particles (Fig. 4). This size differences

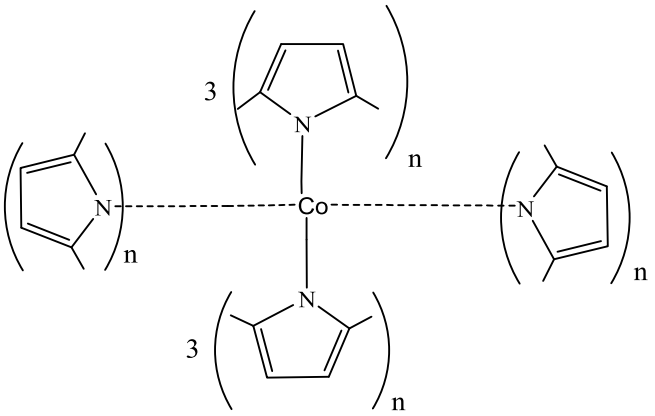

Scheme 1. Proposed active-site structure of CoNPs/PPy.

confirms the incorporation of CoNPs into the PPy in forming the composite. The increased particle sizes in the composite compared with the free CoNPs were due to the interaction of the nanoparticles with the polymer during the growth into larger crystals.

The chemical compositions of CoNPs and CoNPs/PPy were analyzed using EDS (Fig. 5). The EDS peaks of CoNPs showed the presence of Co, Cl, C and O. The Cl atom observed is from the starting material $CoCl_2{\cdot}6H_2O$, C and O were from ethanol used to disperse powder samples for HRTEM analysis. CoNPs/PPy composite is composed of C, O and Co, which confirms that the composite is formed from cobalt nanoparticle and polypyrrole. The absorption peak of copper is attributed to the copper grid used for the characterization of nanoparticles [29].

3.2. Electrochemical characterization

The electrochemical behavior of the electrodes was studied using cyclic voltammetry. The electroactive surface area of the modified electrodes, PPy/GCE, CoNPs/GCE and CoNPs/PPy/GCE were determined in 1.0 mM $[Fe(CN)_6]^{3-/4-}$ in 0.1 M KCl solution at different scan rates. For a reversible process, the Randles-Sevcik formula can be expressed (eqn. (1)):

$$I_p = (2.69 \times 10^5)n^{3/2}ACD^{1/2}v^{1/2} \quad (1)$$

Where, I_p is the peak current, n is the number of electrons transferred (n

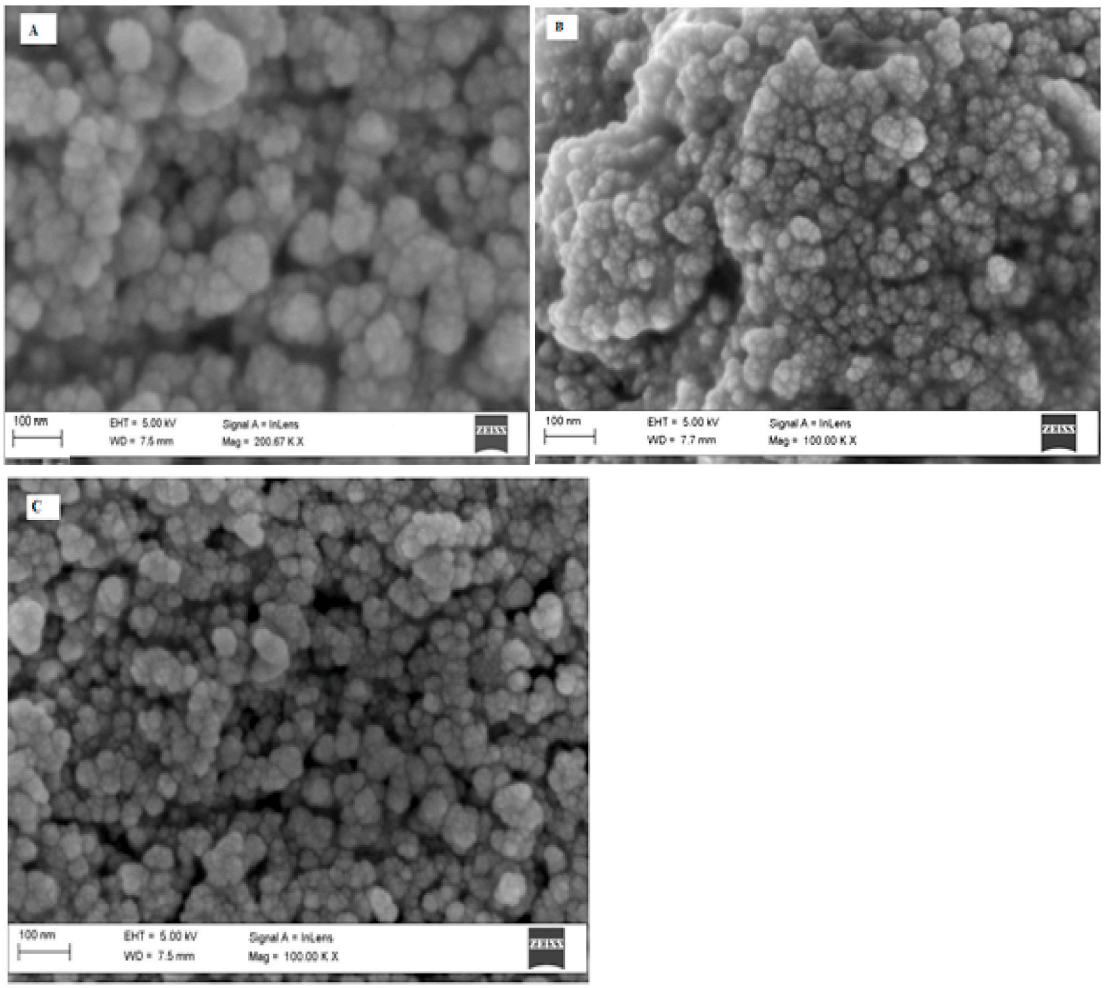

Fig. 3. HRSEM images of PPy (A) CoNPs (B) and CoNPs/PPy (C).

= 1), A is the surface area of the electrode (in cm^2), D is the diffusion coefficient (6.2×10^{-6} cm^2 s^{-1}), ν is the scan rate (in V s^{-1}) and C is the concentration of $[Fe(CN)_6]^{3-/4-}$ (in mol cm^{-3}).

The electroactive surface areas of the electrodes were calculated from the slope of the plot of current *vs* the square root of scan rate. The results showed that the surface area of CoNPs/PPy/GCE was 2.6 and 2.1 times greater than the surface areas of PPy/GCE and CoNPs/GCE, respectively (Table 1). A significant increase in electroactive surface area of CoNPs/PPy/GCE can enhance the sensitivity of the electrode when used for electroanalysis.

3.3. Electrochemical behavior of phoxim

The electrochemical behavior of phoxim was investigated at GCE, PPy/GCE, CoNPs/GCE and CoNPs/PPy/GCE using cyclic volatmmetry. As shown in Fig. 6, a well-defined reduction peak was observed in the absence of any oxidation counterpart, indicating that the electrochemical behavior of phoxim is irreversible. Compared with the bare GCE, increased in the reduction peak current with shift of potential towards positive direction was observed at the surface of PPy/GCE, CoNPs/GCE and CoNPs/PPy/GCE. Furthermore, the decreased in overpotential and increased in the peak current were significant at the surface of CoNPs/PPy/GCE. These remarkable changes indicated that cobalt nanoparticles and polypyrrole have synergistic electrocatalytic effect for the electrochemical reduction of phoxim as a result of their high electroactive surface areas.

Electrochemical impedance spectroscopy (EIS) is an important technique for studying the interfacial properties of the electrode [30]. The electron transfer resistance (R_{ct}) at the surface of the electrode may be related to the diameter of a semicircle and can be used to quantitatively describe the interfacial properties of the electrode [31]. The Nyquist plots consist of a semicircular portion and a linear portion, which correspond to the electron transfer limited process and the diffusion limited process, respectively [32]. Fig. 7 shows the Nyquist plots for bare GCE (a), PPy/GCE (b), CoNPs/GCE (c) and CoNPs/PPy/GCE (d) in 20 μM phoxim solution. It is clearly seen that a bare GCE exhibits large-diameter semicircle, which is the characteristic of a diffusion-limited electrochemical process. Upon modifying the glassy carbon electrode with polypyrrole (PPy/GCE), the diameter (R_{ct}) of Nyquist plot decreased, which is an indication of the increased in the surface roughness and enhanced electron transfer rate which occurred between the electrode and the phoxim. At CoNPs/GCE, the R_{ct} value decreased implying the deposition of highly conductive nanoparticles with high surface area that acted as electron transfer channels. Surprisingly, CoNPs/PPy/GCE, exhibited the smallest electron transfer resistance as compared with the CoNPs/GCE and PPy/GCE. These results support the combined effect of increased surface area and good electrical conductivity of CoNPs/PPy/GCE. The significant change of R_{ct} as a result of modification of GCE indicated that both CoNPs and PPy films have been successfully attached to GCE surface. Thus, the EIS results strongly corroborated the results obtained from the CV study.

Furthermore, the effects of various concentrations of phoxim on the value of charge transfer resistance, R_{ct}, were also studied at the surface of CoNPs/PPy/GCE. The Nyquist plots (Fig. S1A) shows that with

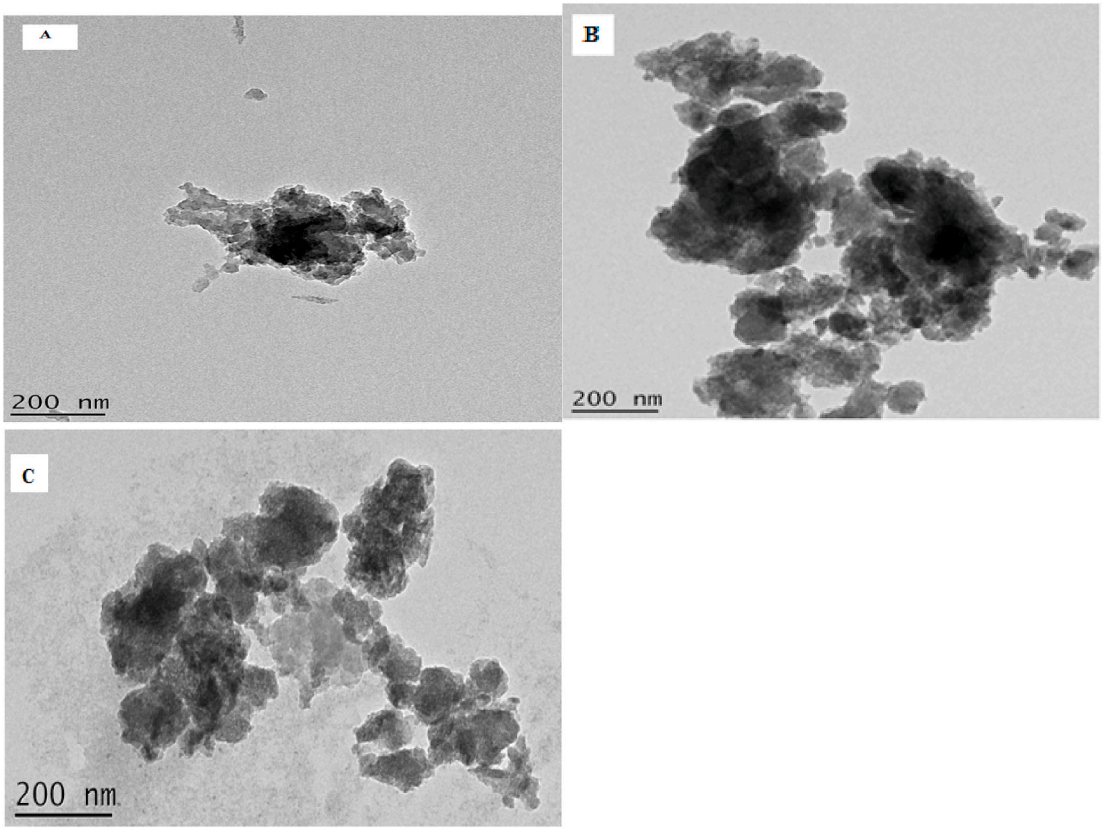

Fig. 4. HRTEM images of PPy (A) CoNPs (B) and CoNPs/PPy (C).

increasing phoxim concentration, the shape of the semicircle began to change and its diameter was gradually decreased. The plot of the reciprocal of charge transfer resistance against the phoxim concentration showed that R_{ct} decreased with increasing phoxim concentration, which indicates that the rate of charge transfer was not hampered with the adsorption of various species on the surface of CoNPs/PPy/GCE.

3.4. Effects of pH

The effect of solution pH on the reduction of phoxim at CoNPs/PPy/GCE was investigated in 0.1 M PBS. From Fig. 8A, it can be observed that the peak current increased as the pH changes from pH 4 to 6 and decreased, then after. As a result, pH 6.0 was selected as the optimum value for subsequent studies. As shown in Equation (2), the peak potential was shifted towards more negative values as the pH increased (Fig. 8B) with a regression equation:

$$E_p(V) = -0.054\ pH + -0.42,\ R^2 = 0.9995 \quad (2)$$

The slope 0.054 V/pH was close to the theoretical value given by the Nernst equation [33], suggesting that the reduction of phoxim involves the transfer of equal number of protons and electrons according to Scheme 2 electrode [12].

3.5. Effects of scan rate

The reaction kinetics of phoxim reduction was investigated by studying the effects of scan rate on the peak current and potential using cyclic voltammetry (Fig. 9A). It can be seen that the reduction peak current increased linearly with an increase in the scan rate in the range 0.05 V s^{-1} - 0.11 V s^{-1} (Fig. 9B) with a regression equation:

$$I_{pc}(\mu A) = -126.1v(V\ s^{-1}) + 1.53,\ R^2 = 0.9970 \quad (3)$$

This indicates that the reduction of phoxim at CoNPs/PPy/GCE is an adsorption-controlled process. Furthermore, the peak potential shifted to more negative values as the scan rate was increased, which further confirming the irreversibility of electrochemical reduction of phoxim [34].

3.6. Effect of accumulation potential and time

In an adsorption controlled process, both accumulation potential and time affect the amount of the adsorbed analyte on the surface of the electrode. The influence of accumulation potential was studied at various applied potentials (−0.2 V to −0.8 V) for a fixed period of time (40 s). The results indicated that the peak current increased from −0.2 V to −0.5 V and decreased when the potential increased beyond −0.5 V (Fig. S2A). Therefore, deposition potential of −0.5 V was taken as the optimum value. The effect of the deposition time on the peak current for phoxim was also studied in the range from 20 s to 70 s. Fig. S2B shows that the peak current increased up to 50 s and then it gradually decreased due to the saturation of the electrode surface. Thus, 50 s was chosen as the optimal accumulation time for further analysis.

3.7. Calibration

Under the optimal conditions, the relationship between peak current and concentration of phoxim was examined using SWV. Fig. 10A shows the SWV responses of the CoNPs/PPy/GCE for various concentrations of phoxim. The peak current increased upon increasing phoxim concentration and a linear response (Fig. 10B) was obtained in the concentration range 0.025 μM–12 μM according to equation (4):

$$I_{pc}(\mu M) = -2.1[phoxim]/\mu M + -5.9,\ R^2 = 0.9984 \quad (4)$$

The limit of detection of the sensor was calculated to be 4.5 nM (S/N = 3).

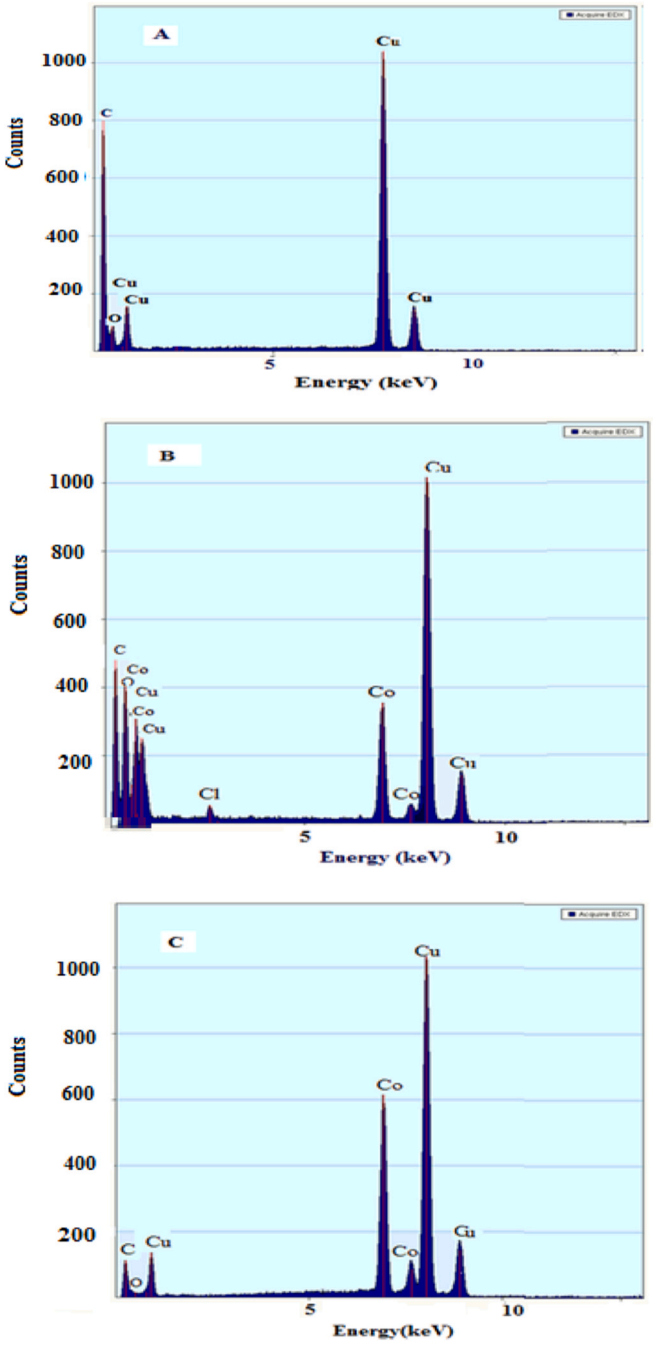

Fig. 5. EDS images of PPy (A) CoNPs (B) and CoNPs/PPy (C).

Table 1
Surface area of the modified electrodes.

Electrode	Surface Area (cm^2)
PPy/GCE	0.125
CoNPs/GCE	0.16
CoNPs/PPy/GCE	0.34

The performance of this sensor was compared with other reported sensors. The linear range and detection limit of the prepared sensor are comparable with or even better than many of previously reported sensors (Table 2). This better performance can be ascribed to the faster electron transfer and high electrocatalytic performance of the sensor as a result of large surface area and good conductivity. Therefore, CoNPs/PPy/GCE could provide a good platform for the effective detection of phoxim.

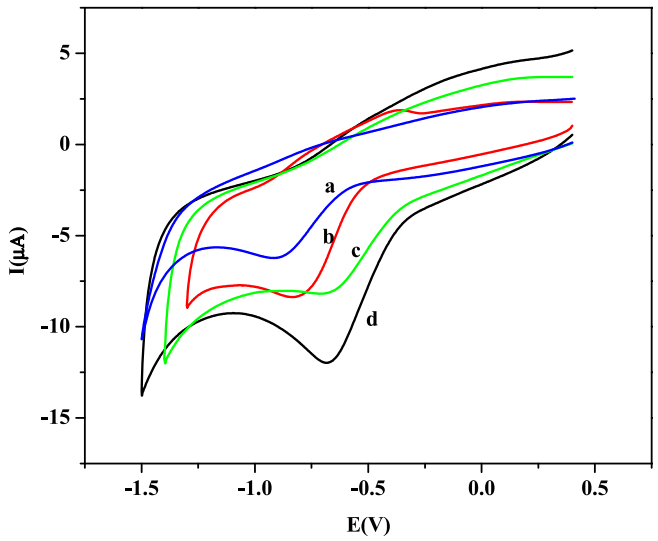

Fig. 6. Cyclic voltammograms of 5 μM phoxim in 0.1 M PBS (pH 7) at GCE (a), PPy/GCE (b), CoNPs/GCE (c) and CoNPs/PPy/GCE (d).

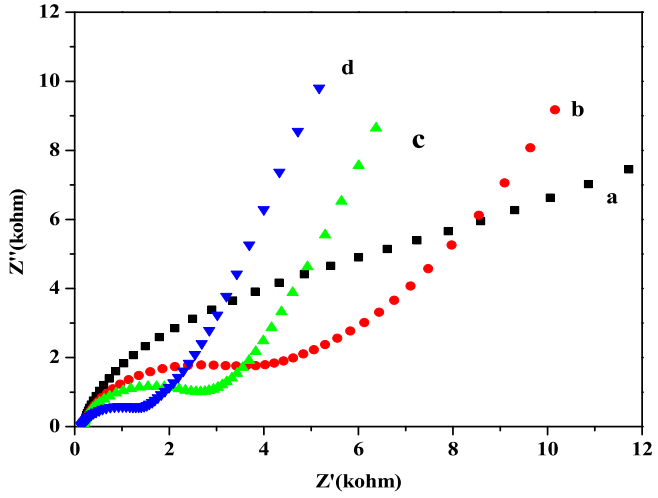

Fig. 7. Nyquist plots of 20 μM phoxim in ethanol for the GCE (a), PPy/GCE (b), CoNPs/GCE (c) and CoNPs/PPy/GCE (d).

3.8. Repeatability, reproducibility and stability of sensor

The repeatability of the CoNPs/PPy/GCE was evaluated with repeated current responses (n = 6) with the same modified electrode for 5 μM phoxim in PBS pH 6 solution and the relative standard deviation (RSD) of the peak current was calculated to be 4.1%. Similarly, the reproducibility of the CoNPs/PPy/GCE was examined by measuring the peak current of phoxim with three different electrodes prepared under the same conditions (n = 5). The relative standard deviation (RSD) of the measurements for the three electrodes was 2.0%, which suggests that the precision and reproducibility of sensor were quite good.

The stability of the sensor was examined after storing it in a refrigerator at 4 °C for 5 days and the peak current was retained 91% of its initial value. This might be the absorption of reduction products which decreases the specific sites. This indicates that the modified electrode has good stability.

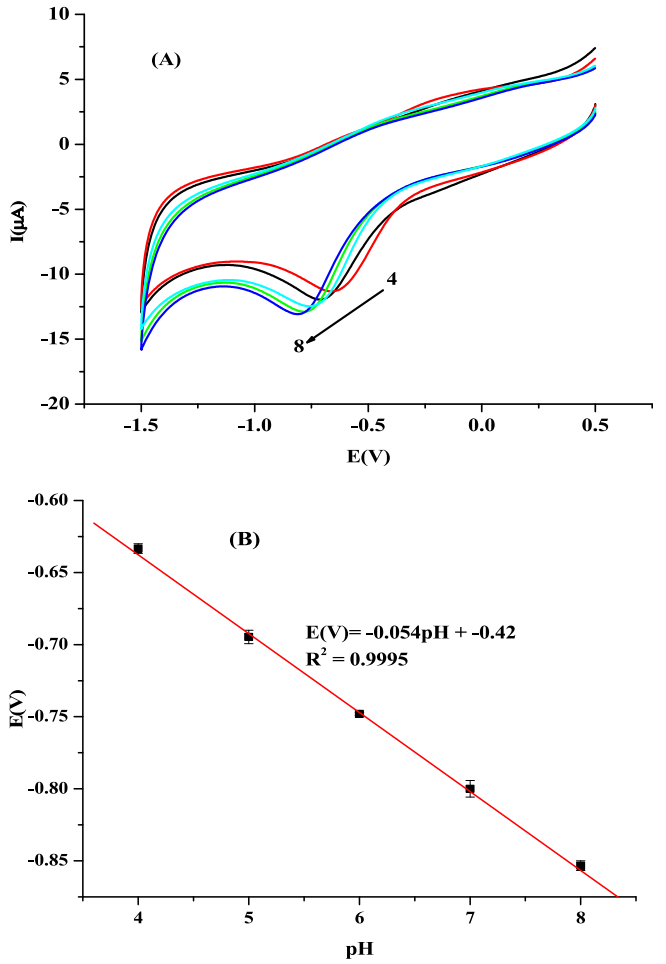

Fig. 8. Effect of pH of PBS on the peak current for 5 μM phoxim at CoNPs/PPy/GCE (A) and plot of peak potential *vs* pH (B).

3.9. Interferences

To apply the proposed method for analytical application, the effects of some common interfering substances such as inorganic ions (Fe^{3+}, Mg^{2+}, Zn^{2+} and Cl^{-}) and pesticides (dichlorvos and phenothrin) in the determination of phoxim were examined by SWV under the optimized conditions. The tolerance limit was defined as the maximum concentration of the interfering substance that caused an error less than 5% in the determination of phoxim [35].

The response of 10 μM phoxim was compared to the response obtained in the presence of these species at various concentrations. The results in Table 3 indicates that 1000-fold of Fe^{3+}, Mg^{2+}, Zn^{2+} and Cl^{-} did not interfere with the determination of phoxim. 10-fold of dichlorvos and phenothrin did not influence the current responses of phoxim. Change of ±5% in the phoxim peak current in the presence of interferents proved the sensor had good selectivity.

3.10. Analytical application

Under the optimum conditions, CoNPs/PPy/GCE was applied for the determination of phoxim in water samples. After the pH of the water sample was adjusted with 0.1 M PBS of pH 6.0, the water sample was analyzed first without addition of phoxim standard. As can be seen in Fig. S3, no voltammeteric response which corresponds to phoxim was observed when the water samples were analyzed. Subsequently, the water samples were spiked with various concentrations of phoxim (0.75, 2, 4 and 6 μM). The recovery of the water samples were ranged from 94.6% to 100.2% (Table 4), indicating that the sensor could be successfully applied for phoxim determination in real samples with good recovery.

4. Conclusion

We have developed a simple and sensitive electrochemical sensor based on CoNPs/PPy/GCE. Due to the combination of the unique properties of nanoparticles and the polymer, the CoNPs/PPy/GCE

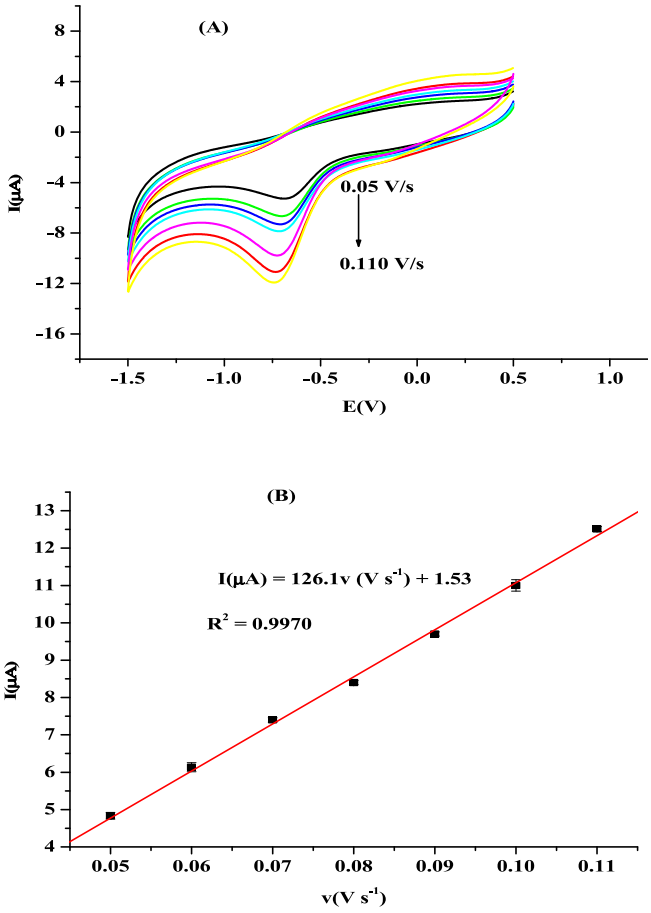

Fig. 9. Cyclic voltammograms for 5.0 μM phoxim in 0.1 M PBS pH 6.0 at the CoNPs/PPy/GCE at various scan rates (A) and plot of the peak current *vs* scan rates (B).

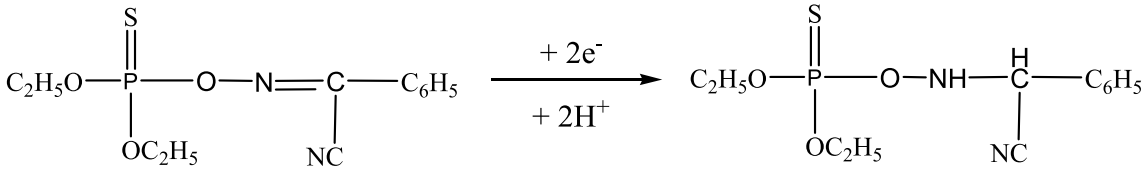

Scheme 2. Mechanism of phoxim reduction.

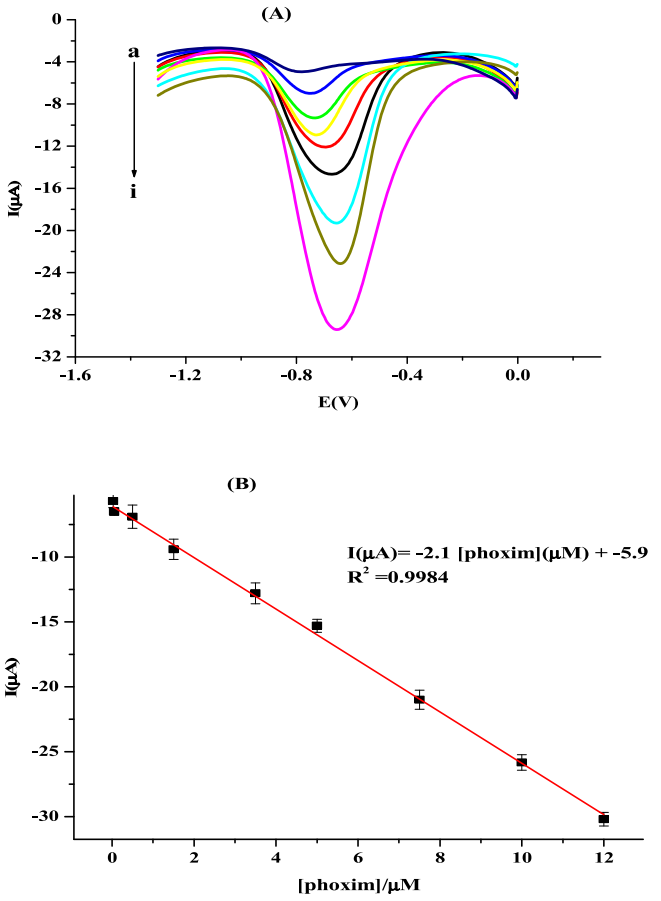

Fig. 10. (A) Square wave voltammograms for various concentrations of phoxim in PBS pH 6.0 at CoNPs/PPy/GCE electrode: (a) 0.025, (b) 0.05, (c) 0.5, (d) 1.5, (e) 3.5, (f) 5.0, (g) 7.5, (h) 10 and (i) 12 μM. (B) calibration plot of peak current with concentrations of phoxim at CoNPs/PPy/GCE.

Table 2
Comparison of different electrochemical sensors reported for the determination of phoxim.

Electrodes	Linear range (μM)	Detection limit(nM)	References
Gr/GCE	0.02–20	8.01	12
AuNPs/RGO/GCE	0.01–10	3	13
P3MT/NGE/GCE	0.02–0.2	6.4	14
MIP/graphene/GCE	0.8–140	20	15
CoNPs/PPy/GCE	0.025–12	4.5	This work

Gr: Graphene.
AuNPs/RGO: Gold nanoparticles-reduced graphene oxide.
P3MT/NGE: poly(3-methylthiophene)/nitrogen doped graphene.
MIP: molecular imprinted.

Table 3
Influence of potential interferences on the voltammetric response of CoNPs/PPy/GCE to 10 μM phoxim.

Interference	Concentration (mM)	Signal change (%)
Fe^{3+}	10	+1.5
Mg^{2+}	10	−2.7
Zn^{2+}	10	−4.7
Cl^{-}	10	−2.6
Dichlorvos	0.1	−4.7
Phenothrin	0.1	−4.4

Table 4
Determination of phoxim in river water sample.

Sample	Amount added (μM)	Amount found[a] (μM)	Recovery (%)
Water	0.75	0.71 ± 0.13	94.6
	2.0	1.9 ± 0.69	95.0
	4.0	3.85 ± 0.20	96.3
	6.0	6.01 ± 0.29	100.2

[a] Mean of triplicate measurements±sd.

electrode showed peak currents enhancement and decrease in the peak potentials. The sensor exhibited excellent reproducibility and good stability. Furthermore, the selectivity of CoNPs/PPy/GCE towards phoxim was investigated in the presence of different interfering species and no significant interference was noted. Lastly, the proposed method showed satisfactory results when applied for the determination of phoxim using square wave voltammetry in river water samples with good precision and recoveries.

CRediT authorship contribution statement

Molla Tefera: Data curation, Investigation, Writing – original draft. **Merid Tessema:** Writing – review & editing. **Shimelis Admassie:** Conceptualization, designed the experiments. **Meryck Ward:** Software, Validation. **Lisebo Phelane:** Software, Validation. **Emmanuel I. Iwuoha:** Supervision. **Priscilla G.L. Baker:** Supervision.

Declaration of competing interest

The authors declare that they have no known competing financial interests or personal relationships that could have appeared to influence the work reported in this paper.

Appendix A. Supplementary data

Supplementary data to this article can be found online at https://doi.org/10.1016/j.acax.2021.100077.

References

[1] M. Facure, L. Mercante, L. Mattoso, D. Correa, Detection of trace levels of organophosphate pesticides using an electronic tongue based on graphene hybrid nanocomposites, Talanta 167 (2017) 59–66.
[2] M. Khairy, H. Ayoub, C. Banks, Non-enzymatic electrochemical platform for parathion pesticide sensing based on nanometer-sized nickel oxide modified screen-printed electrodes, Food Chem. 255 (2018) 104–111.
[3] H. Sapahin, A. Makahleh, B. Saad, Determination of organophosphorus pesticide residues in vegetables using solid phase micro-extraction coupled with gas chromatography–flame photometric detector, Arabian J. Chem. 12 (2019) 1934–1944.
[4] S. Fuhrimann, A. Farnham, P. Staudacher, A. Atuhaire, T. Manfioletti, C. Niwagaba, S. Namirembe, J. Mugweri, M. Winkler, L. Portengen, H. Kromhout, A. Mora, Exposure to multiple pesticides and neurobehavioral outcomes among smallholder farmers in Uganda, Environ. Int. 152 (2021) 1–10.
[5] C. Hyland, K. Kogut, R. Gunier, R. Castorina, C. Curl, B. Eskenazi, A. Bradman, Organophosphate pesticide dose estimation from spot and 24-hr urine samples collected from children in an agricultural community, Environ. Int. 146 (2021) 1–11.
[6] N. Pugliese, E. Circella, G. Cocciolo, A. Giangaspero, D. Tomic, T. Kika, A. Caroli, A. Camarda, Efficacy of λ-cyhalothrin, amitraz, and phoxim against the poultry red mite Dermanyssus gallinae De Geer, 1778 (Mesostigmata: dermanyssidae), Avian Pathol. 48 (2019) 35–43.
[7] X. Qin, X. Luo, Y. Chen, J. Han, J. Zhang, K. Zhang, D. Hu, A liquid chromatography–tandem mass spectrometry method to simultaneously determinate dichlorvos and phoxim in tobacco, Biomed. Chromatogr. 33 (2019) 1–15.
[8] F. Tian, X. Liu, J. Xu, F. Dong, Y. Zheng, M. Hu, Y. Wu, Simultaneous determination of phoxim, chlorpyrifos, and pyridaben residues in edible mushrooms by high-performance liquid chromatography coupled to tandem mass spectrometry, Food Anal. Methods 9 (2016) 2917–2924.
[9] B. Perez-Fernandez, A. Costa-García, A. Escosura- Muñiz, Electrochemical (Bio) sensors for pesticides detection using screen-printed electrodes, Biosensors 10 (2020) 1–26.

[10] M. Tefera, M. Tessema, S. Admassie, E. Iwuohac, T. Waryo, P. Baker, Electrochemical determination of phenothrin in fruit juices at graphene oxide-polypyrrole modified glassy carbon electrode, Sens. Biosensing Res. 21 (2018) 27–34.
[11] H. Yin, S. Ai, J. Xu, W. Shi, L. Zhu, Amperometric biosensor based on immobilized acetylcholinesterase on gold nanoparticles and silk fibroin modified platinum electrode for detection of methyl paraoxon, carbofuran and phoxim, J. Electroanal. Chem. 637 (2009) 21–27.
[12] M. Chao, M. Chen, Electrochemical determination of phoxim in food samples employing a graphene-modified glassy carbon electrode, Food Anal. Methods 7 (2014) 1729–1736.
[13] Y. Zheng, A. Wang, H. Lin, L. Fu, W. Cai, A sensitive electrochemical sensor for direct phoxim detection based on an electrodeposited reduced graphene oxide–gold nanocomposite, RSC Adv. 5 (2015) 15425–15430.
[14] L. Wu, W. Lei, Z. Han, Y. Zhang, M. Xia, Q. Hao, A novel non-enzyme amperometric plat form based on poly(3-methylthiophene)/nitrogen doped graphene modified electrode for determination of trace amounts of pesticide phoxim, Sensor. Actuator. B 206 (2015) 495–501.
[15] X. Tan, J. Wu, Q. Hu, X. Li, P. Li, H. Yu, X. Li, F. Lei, An electrochemical sensor for the determination of phoxim based on a graphene modified electrode and molecularly imprinted polymer, Anal Methods 7 (2015) 4786–4792.
[16] F. Xu, Z. Cui, H. Li, Y. Luo, Electrochemical determination of trace pesticide residues based on multiwalled carbon nanotube grafted acryloyloxy ferrocene carboxylates with different spacers, RSC Adv. 7 (2017) 7431–7441.
[17] M. Naveen, N. Gurudatt, Y. Shim, Applications of conducting polymer composites to electrochemical sensors, Appl. Mater. Today. 9 (2017) 419–433.
[18] S. Ramanavicius, A. Ramanavicius, Conducting polymers in the design of biosensors and biofuel cells, Polymers 13 (2021) 1–19.
[19] M. Rhazi, S. Majid, ·M. Elbasri, F. Salih, L. Oularbi, K. Lafdi, Recent progress in nanocomposites based on conducting polymer: application as electrochemical sensors, Int. Nano Lett. 8 (2018) 79–99.
[20] F. Nejad, S. Tajik, H. Beitollahi, I. Sheikhshoaie, Magnetic nanomaterials based electrochemical (bio)sensors for food analysis, Talanta 228 (2021) 1–23.
[21] S. Tajik, H. Beitollahi, H. Jang, M. Shokouhimehr, A screen printed electrode modified with Fe_3O_4@polypyrrole-Pt core-shell nanoparticles for electrochemical detection of 6-mercaptopurine and 6-thioguanine, Talanta 232 (2021) 1–7.
[22] S. Tajik, H. Beitollahi, F. Nejad, Z. Dourandish, M. Khalilzadeh, H. Jang, R. Venditti, R. Varma, M. Shokouhimehr, Recent developments in polymer nanocomposite-based electrochemical sensors for detecting environmental pollutants, Ind. Eng. Chem. Res. 60 (2021) 1112–1136.
[23] L. Phelane, F. Muya, H. Richards, P. Baker, E. Iwuoha, Polysulfone nanocomposite membranes with improved hydrophilicity, Electrochim. Acta 128 (2014) 326–335.
[24] E. Hess, T. Waryo, O. Sadik, E. Iwuoha, P. Baker, Constitution of novel polyamic acid/polypyrrole composite films by in-situ electropolymerization, Electrochim. Acta 128 (2014) 439–447.
[25] C. Merlini, B. Rosa, D. Muller, L. Ecco, S. Ramoa, G. Barra, Polypyrrole nanoparticles coated amorphous short silica fibers: synthesis and characterization, Polym. Test. 31 (2012) 971–977.
[26] N. Su, H. Li, S. Yuan, S. Yi, E. Yin, Synthesis and characterization of polypyrrole doped with anionic spherical polyelectrolyte brushes, Polym. Lett. 6 (2012) 697–705.
[27] K. Ghanbari, N. Hajheidari, Simultaneous electrochemical determination of dopamine, uric acid and ascorbic acid using silver nanoparticles deposited on polypyrrole nanofibers, J. Polym. Res. 22 (2015) 1–9.
[28] Z. Shi, H. Liu, K. Lee, E. Dy, J. Chlistunoff, M. Blair, P. Zelenay, J. Zhang, Z. Liu, Theoretical study of possible active site structures in cobalt-polypyrrole catalysts for oxygen reduction reaction, J. Phys. Chem. C 115 (2011) 16672–16680.
[29] K. Sethi, I. Roy, Organically modified titania nanoparticles for sustained drug release applications, J. Colloid Interface Sci. 456 (2015) 59–65.
[30] P. Calvo, O. Campo, C. Guerra, S. Castano, F. Fonthal, Design of using chamber system based on electrical impedance spectroscopy (EIS) to measure epithelial tissue, Sens. Biosensing Res. 29 (2020) 1–9.
[31] Y. Hartatia, S. Gaffara, D. Alfiani, U. Pratomo, Y. Sofiatin, T. Subroto, Voltammetric immunosensor based on gold nanoparticle -Anti-ENaC bioconjugate for the detection of epithelial sodium channel (ENaC) protein as a biomarker of hypertension, Sens. Biosensing Res. 29 (2020) 1–8.
[32] P. Bujewska, B. Gorska, K. Fic, Redox activity of selenocyanate anion in electrochemical capacitor application, Synth. Met. 253 (2019) 62–72.
[33] G. Fadillah, S. Triana, U. Chasanah, T. Saleh, Titania-nanorods modified carbon paste electrode for the sensitive voltammetric determination of BPA in exposed bottled water, Sens. Biosensing Res. 30 (2020) 1–9.
[34] M. Amare, W. Teklay, Voltammetric determination of paracetamol in pharmaceutical tablet samples using anthraquinone modified carbon paste electrode, Cogent Chem 5 (2019) 1–10.
[35] J. Gowda, S. Nandibewoor, Electrochemical characterization and determination of paclitaxel drug using graphite pencil electrode, Electrochim. Acta 116 (2014) 326–333.